Biochimica et Biophysica Acta 1817 (2012) 1072–1082

Contents lists available at SciVerse ScienceDirect

Biochimica et Biophysica Acta

journal homepage: www.elsevier.com/locate/bbabio

Substrate-dependent modulation of the enzymatic catalytic activity: Reduction of nitrate, chlorate and perchlorate by respiratory nitrate reductase from *Marinobacter hydrocarbonoclasticus* 617

Jacopo Marangon [a], Patrícia M. Paes de Sousa [a], Isabel Moura [a], Carlos D. Brondino [b], José J.G. Moura [a,*], Pablo J. González [a,*]

[a] *REQUIMTE, Departamento de Química, Centro de Química Fina e Biotecnologia, Faculdade de Ciências e Tecnologia, Universidade Nova de Lisboa, 2829-516 Caparica, Portugal*
[b] *Departamento de Física, Facultad de Bioquímica y Ciencias Biológicas, Universidad Nacional del Litoral, S3000ZAA Santa Fe, Argentina*

ARTICLE INFO

Article history:
Received 20 December 2011
Received in revised form 23 March 2012
Accepted 17 April 2012
Available online 25 April 2012

Keywords:
Nitrate reductase
Molybdenum
Denitrification
Protein film voltammetry
Enzyme catalysis

ABSTRACT

The respiratory nitrate reductase complex (NarGHI) from *Marinobacter hydrocarbonoclasticus* 617 (*Mh*, formerly *Pseudomonas nautica* 617) catalyzes the reduction of nitrate to nitrite. This reaction is the first step of the denitrification pathway and is coupled to the quinone pool oxidation and proton translocation to the periplasm, which generates the proton motive force needed for ATP synthesis. The *Mh* NarGH water-soluble heterodimer has been purified and the kinetic and redox properties have been studied through in-solution enzyme kinetics, protein film voltammetry and spectropotentiometric redox titration. The kinetic parameters of *Mh* NarGH toward substrates and inhibitors are consistent with those reported for other respiratory nitrate reductases. Protein film voltammetry showed that at least two catalytically distinct forms of the enzyme, which depend on the applied potential, are responsible for substrate reduction. These two forms are affected differentially by the oxidizing substrate, as well as by pH and inhibitors. A new model for the potential dependence of the catalytic efficiency of Nars is proposed.

1. Introduction

Because of their respiratory flexibility, bacteria can utilize a diverse range of electron acceptors such as oxygen, nitrogen oxyanions and oxides, elemental sulfur and sulfur oxyanions, within others. This respiratory diversity contributes to the ability of prokaryotes to colonize many of Earth's most hostile microoxic and anoxic environments [1]. A good example of respiratory flexibility can be found in *Marinobacter hydrocarbonoclasticus* 617 (*Mh*, formerly known as *Pseudomonas nautica* 617), a marine bacterium that besides aerobic respiration can develop a complete denitrification pathway under denitrifying conditions (anaerobiosis and a small amount of nitrate). In this pathway, the nitrate reduction is a way to consume the reducing equivalents generated by the metabolism, a role played by dioxygen in aerobic respiration. During the growth in micro-aerobic or anaerobic environments nitrate can be exploited as respiratory substrate, contributing to the generation of the proton motive force across the cytoplasmic membrane [2–5]. The nitrate reductase (NR) responsible for this process in *Mh* catalyzes the first step of the denitrification pathway, i.e., reduction of nitrate to nitrite according to the reaction:

$$NO_3^- + 2H^+ + 2e^- \rightarrow NO_2^- + H_2O \qquad E^0 = 420 \text{ mVvs.SHE} \qquad (1)$$

Mh respiratory nitrate reductase (Nar) is a membrane-bound heterotrimer protein belonging to the DMSO reductase family of mononuclear Mo enzymes closely related to the Nar from *Escherichia coli* K12 (*Ec*) and *Paracoccus pantotrophus* GB17 (*Pp*) [6,7]. These proteins have a flower-like arrangement composed by two cytoplasmic subunits, NarG (112–140 kDa) and NarH (52–64 kDa), and a membrane subunit NarI (19–25 kDa) that is entirely buried into the phospholipids bilayer (Fig. 1a) [2]. These enzymes can be purified as a detergent-solubilized heterotrimer (NarGHI) or in a two-subunit water-soluble form (NarGH), which is also catalytically competent [8–10]. The largest subunit NarG contains the active site and a [4Fe–4S] cluster (FS0) (Fig. 1b) [11,12]. The Mo ion is coordinated by four thiolates of two pyranopterin molecules, forming the molybdopterin guanine dinucleotide cofactor (Mo-*bis*PGD). The crystal structures of *Ec* NarGHI and *Ec* NarGH revealed that the side-chain carboxylate of Asp222 coordinates the Mo ion in a bidentate fashion in the heterotrimer and monodentate in the heterodimer with the sixth coordination position being occupied by an oxo group, which is absent in the heterotrimer [13,14]. Since crystals of both NarGHI and NarGH were grown under

Abbreviations: Nar, respiratory nitrate reductase; Nap, periplasmic nitrate reductase; NR, nitrate reductase; *Mh*, *Marinobacter hydrocarbonoclasticus* 617; *Ec*, *Escherichia coli* K12; *Pp*, *Paracoccus pantotrophus* GB17; *Pd*, *Paracoccus denitrificans* NCIMB 6944; PFV, protein film voltammetry; EPR, electron paramagnetic resonance; SHE, standard hydrogen electrode

* Corresponding authors. Tel.: +351 212948300x10967; fax: +351 212948385.
E-mail addresses: jose.moura@fct.unl.pt (J.J.G. Moura), p.gonzalez@fct.unl.pt (P.J. González).

0005-2728/$ – see front matter © 2012 Published by Elsevier B.V.
doi:10.1016/j.bbabio.2012.04.011

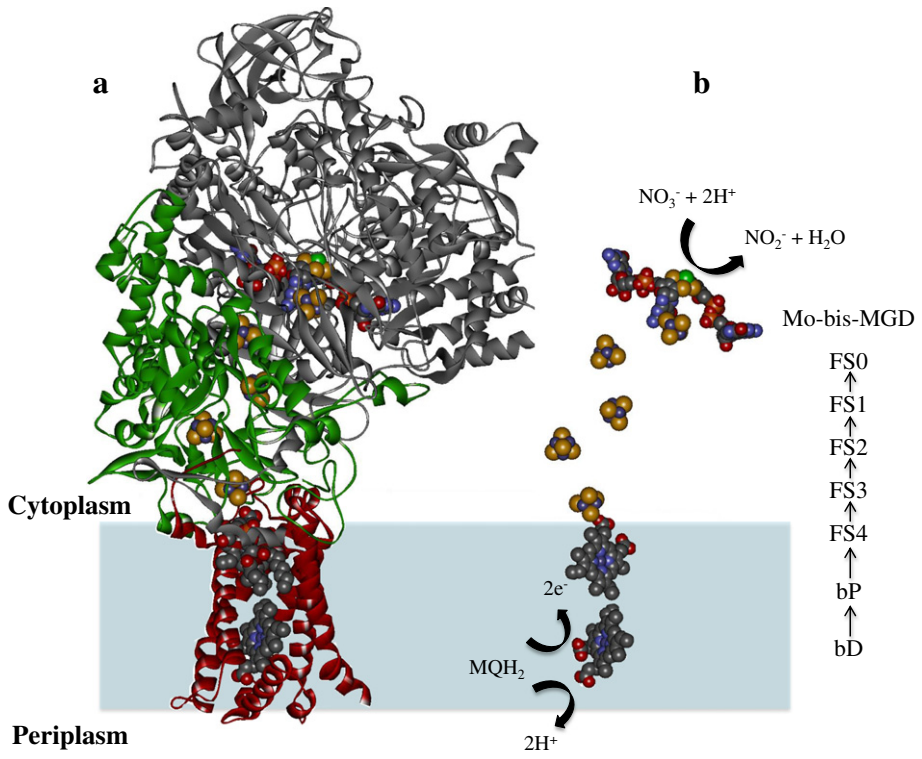

Fig. 1. (a) Crystallographic structure of the *Ec* NarGHI heterotrimer anchored to the cytoplasmic membrane through the NarI subunit (red). The NarGH subunits (gray and green) are located in the bacterial cytoplasm. (b) The redox cofactors of the electron transfer pathway of NarGHI comprise two *b*-type hemes that gather electrons from the quinone pool, one [3Fe–4S] and four [4Fe–4S] clusters, and the Mo-*bis*-PGD where the reduction of nitrate to nitrite occurs.

aerobic conditions, it was concluded that in both coordination modes the Mo ion is in the oxidized VI state. Furthermore, the structure of *Ec* NarGHI showed that one of the pterins presents an open bicyclic configuration, which probably undergoes a reversible cyclization during catalysis [13]. The NarH subunit contains one [3Fe–4S] cluster (FS4) and three [4Fe–4S] clusters (FS3, FS2, and FS1) and the small NarI subunit contains two *b*-type hemes (Fig. 1b). All the redox cofactors in the heterotrimer are aligned in a single chain within the distance for electron transfer [13,14], allowing the communication between the Mo active site in NarG with the distal *b*-type heme in NarI. The electron physiological donor for nitrate reduction is the membrane quinol pool. The NarI subunit is the site for quinol oxidation, process in which protons are translocated to the periplasm while electrons are directed through the redox cofactors toward the Mo active site. This mechanism imply that quinol oxidation and nitrate reduction occur at separate sites on the enzyme, in agreement with studies that showed that the kinetic behavior of the quinol–nitrate oxidoreductase activity is consistent with a two-site enzyme substitution mechanism [9].

The reaction mechanism of *Ec* and *Pp* Nars has been extensively studied by means of in-solution enzyme kinetics and protein film voltammetry (PFV). These studies gave new insights on how the catalytic reduction of nitrate occurs at the Mo active site of these enzymes. All PFV studies showed two-component electrochemical responses that were interpreted in different ways as a potential-dependent activity of Nar [15,16]. Based on the data obtained for *Pp* NarGH, Anderson et al. [15] proposed a scheme for substrate interaction and reduction where the Mo(IV):nitrate complex can be achieved via two kinetically distinct pathways (Scheme 1).

In the first pathway, the Mo(VI) ion is one-electron reduced to Mo(V), then nitrate binds and a subsequent one-electron reduction of the metal center will provide the electron needed to complete the redox reaction. In the second pathway, the Mo(VI) ion is two-electron reduced to Mo(IV), then nitrate binds and it is immediately reduced. Based on this scheme, the authors proposed that the preferential pathway would be determined by the rate of electron and substrate addition to the active site. This model was used to explain the substrate concentration-dependence of the waveshape of the catalytic voltammograms of *Pp* NarGH [15]. It was observed that at low substrate concentrations the waveshapes are characterized by a local maximum that disappears at substrate saturating conditions. This behavior was explained assuming that catalysis via Mo(IV):nitrate complex proceeds with a lower specificity constant compared to the catalysis via Mo(V):nitrate. Moreover, at higher substrate concentrations the kinetic distinction between both pathways is lost as the catalysis becomes enzyme-limited, yielding a sigmoidal catalytic waveshape. PFV data obtained for *Ec* NarGHI was interpreted in a different way by Elliott et al. [16]. The catalytic waves obtained for the heterotrimer were characterized by two distinct activities at high and low potential, respectively. The K_M values obtained for these activities were different, indicating a potential dependence of the nitrate binding affinity. This evidence supported the proposal that the Mo center plays an important role in determining the current-potential profile, making unlikely other contributions such as an influence of the oxidation

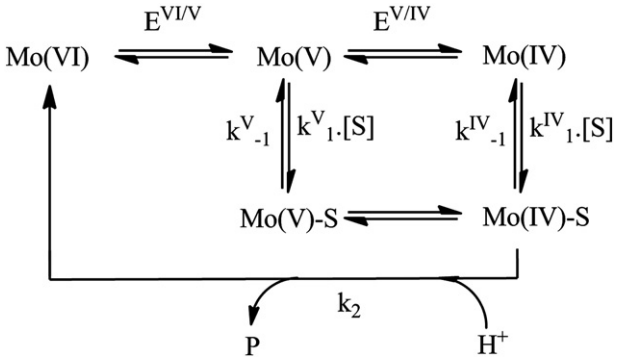

Scheme 1. Mechanism of nitrate reduction based on voltammetric evidences, proposed by Anderson et al. [15] and Elliot et al. [16] for *Pp* NarGH and *Ec* NarGHI respectively.

state of the Fe–S clusters, resulting in the existence of two distinct active conformations of the enzyme on the electrode [16].

To gain further insight into the reaction mechanism of respiratory nitrate reductases, we report in-solution enzyme kinetic, spectropotentiometric redox titration, and PFV studies in *Mh* NarGH. The kinetic and PFV studies were performed in the presence of nitrate, alternative substrates, and inhibitors. Although the potential-dependent activity of *Mh* NarGH is similar in several aspects to those observed for *Ec* NarGHI and *Pp* NarGH, the results obtained with alternative substrates suggest a rather different catalytic scheme, which gives an alternative explanation for the two-component electrochemical response.

2. Materials and methods

2.1. Cells growth and NarGH purification

Marinobacter hydrocarbonoclasticus 617 (*Mh*) was grown under denitrifying conditions in artificial seawater at 303 K with 10 mM nitrate as electron acceptor [17,18]. The NarGH was purified using a heat treatment protocol in order to release the heterodimer from the membrane fraction as reported by Correia et al. [10]. Briefly, the membrane fraction of *Mh* obtained after ultracentrifugation of the crude extract presented nitrate reductase activity and was used as source for the purification of the heat-solubilized NarGH heterodimer. SDS-PAGE of the as-isolated NarGH obtained after three chromatographic columns showed two bands with respective molecular masses of *ca.* 140 and 58 kDa. These molecular masses are similar to those determined for NarGH from *E. coli* K12 and *P. pantotrophus* GB17 [6,7]. The UV–visible spectrum of the oxidized *Mh* NarGH showed the typical broad shoulder around 400 nm, characteristic of the Fe–S centers absorption. The sample used for these studies presented a high purity ratio deduced from UV–vis spectroscopy (A_{400}/A_{280} ~4).

2.2. Spectrophotometric kinetic assays

Nitrate reduction was monitored following the oxidation of the artificial donor methyl viologen at 604 nm ($\varepsilon_{604} = 13.6\ mM^{-1}\ cm^{-1}$, Sigma) as reported by Craske et al. [8] using a TIDAS/NMC301-MMS/16 VIS/500-1 diode array spectrophotometer (J&M, Analytische Mess und Regeltechnik, Aalen, Germany). The data were acquired and analyzed using the BioKine32 software. The total volume of the reaction mixture was 1 ml and comprised 100 mM Tris–HCl 7.60 and 1 mM methyl viologen. Sodium dithionite was added till one unit of absorbance was obtained. The reaction was started by adding potassium nitrate, chlorate, or perchlorate at the desired concentration. Nitrate reductase specific activity is expressed in micromoles of nitrate reduced per minute per milligram of enzyme (U/mg). All measurements were performed in a glovebox (O_2<1 ppm) and in quartz cells (1 ml) provided with magnetic stirrers.

2.3. Electrochemical measurements

Cyclic voltammetry was performed on a potentiostat μAUTOLAB Type III (Eco Chemie, Utrecht, The Netherlands). The data were collected using the GPES (Eco Chemie) software package. All the reagents and the buffer–electrolytes were of analytical grade (Merck and Panreac) and were prepared using Milli-Q water of resistivity 18 MΩ·cm. An all-glass cell with a three-electrode configuration was employed for voltammetry. The cell was housed in an anaerobic glovebox (Argon atmosphere, O_2<1 ppm). A pyrolytic graphite (PG) rotating disk electrode (RDE) was used combined with the CTV101 Speed Control Unit (Radiometer Analytical). The counter electrode was a platinum wire, and the reference electrode was an Ag/AgCl (3.5 M KCl) electrode. All potentials were corrected versus standard hydrogen electrode (SHE) using $E_{SHE} = E_{Ag/AgCl} + 205$ mV at room temperature [19]. The PG electrode was polished with 1.0, 0.3 and 0.05 μm water alumina slurry (Buehler), sonicated in water and then smeared with 2 μl of enzyme solution (~30 μM NarGH) in 10 mM Tris–HCl buffer, pH 7.60, containing 2 mM neomycin (Fluka). The electrode was rotated at 2000 rpm, and the potential was cycled at a scan rate of 0.02 V/s. The electrolyte used was 10 mM Tris–HCl buffer, pH 7.60. Under these conditions it was possible to record several catalytic responses for different substrate concentrations using the same film.

2.4. Spectropotentiometric redox titration

EPR mediated redox titrations were carried out in an anaerobic glovebox at room temperature working at an oxygen concentration below 1 ppm. A platinum–silver/silver chloride combined electrode (Crison) calibrated with a reference standard buffer, pH 7.00 (SIGMA), and saturated with quinhydrone was used to determine the electrochemical potential of the solution. The protein solution (~150 μM) was incubated with the mediators dyes (5 μM each): methylene blue (11 mV), resorufin (−51 mV), indigo disulphate (−125 mV), di-hydroxy 1,4-naphtoquinone (−145 mV), phenosafranin (−225 mV), and benzyl viologen (−340 mV). The electrochemical potential was dropped using a sodium dithionite solution dissolved in 10 mM Tris–HCl, pH 7.60. Samples for EPR spectroscopy (100 μl) were taken after equilibration at each potential and frozen in liquid nitrogen. Values of redox potentials are expressed relative to the standard hydrogen electrode (SHE). X-band EPR spectra were recorded using a Bruker EMX spectrometer equipped with rectangular dual mode cavity (model EPR 4102ST) and a helium continuous flow cryostat (Oxford Instruments).

3. Results

3.1. Spectrophotometric kinetic studies in solution

The heat-solubilized form of the enzyme (NarGH) showed a specific activity of 16 U/mg. The activity vs. pH profile of *Mh* NarGH showed that the activity is constant between pH 6.00 and 8.00, dropping significantly above pH 8.00 (data not shown). For this reason, all kinetic studies were performed at pH 7.60, a pH value in which the enzyme presents good stability.

The catalytic properties of *Mh* NarGH were studied using stereochemically distinct substrates: nitrate (planar), chlorate (pyramidal) and perchlorate (tetrahedral). The active site of respiratory nitrate reductases present a high flexibility, making them able to catalyze the reduction of anions with geometries different from that of nitrate, as have been described already for *Ec* NarGHI, *Pd* NarGHI and *Pp* NarGH [8,9,15]. This is in contrast with periplasmic nitrate reductases, which are highly specific toward trigonal planar nitrate molecules. The kinetic data of reduction of nitrate, chlorate and perchlorate of *Mh* NarGH were analyzed assuming a Michaelis–Menten model. The kinetic constants K_M and k_{cat} for these three substrates were obtained through the direct linear plot analysis and are summarized in Table 1. The Michaelis constant determined for nitrate (K_M = 225 μM) is very similar to those obtained for *Ec* NarGHI (K_M = 420 μM) [9], *Pd* NarGHI (K_M = 283 μM) [8], and *Pp* NarGH. *Pp* NarGH yields kinetic constants very similar to those of *Pd* NarGHI (J. Butt, personal communication). For *Mh* NarGH, the K_M values for chlorate and perchlorate are about seven-fold larger than for nitrate.

Table 1
K_M, k_{cat} and K_i (N_3^-) values determined by in-solution enzyme kinetics for NO_3^-, ClO_3^- and ClO_4^- with reduced methyl viologen as electron donor to nitrate reductase. nd, not determined.

NarGH	K_M [μM]	k_{cat} [s^{-1}]	k_{cat}/K_M [s^{-1}/μM]	K_{iC} [μM] (N_3^-)	K_{iU} [μM] (N_3^-)
NO_3^-	225	355	1.58	0.9	3.1
ClO_3^-	1677	579	0.35	nd	nd
ClO_4^-	1471	18	0.01	nd	nd

Morpeth et al. [9] reported that the turnover rate of *Ec* NarGHI for chlorate ($700\ s^{-1}$) is higher than the value obtained for nitrate ($450\ s^{-1}$) yielding a k_{cat} (chlorate)/k_{cat} (nitrate) ratio of 1.55. A similar ratio between these turnover rates was obtained for *Mh* NarGH (1.63). Nevertheless, despite the k_{cat} for chlorate being almost the double of that obtained for nitrate, the k_{cat}/K_M ratios indicate that *Mh* NarGH is ca. five-fold more specific for nitrate than chlorate (Table 1). The k_{cat}/K_M ratio for perchlorate is significantly smaller than those of nitrate and chlorate, suggesting very poor affinity of *Mh* NarGH for this bulky anion.

The inhibitory properties of azide in *Mh* NarGH were also investigated. The analysis of Dixon and Cornish plots (used to determine the competitive and uncompetitive constants, respectively) showed that azide is a mixed inhibitor of the nitrate reduction when reduced methyl viologen is used as electron donor (Fig. S1a). The K_{iC} and K_{iU} values presented in Table 1 indicated that azide is a strong inhibitor, as also observed in *Ec* NarGHI [16]. In addition, K_{iC} (competitive) is three-fold smaller than K_{iU} (uncompetitive), indicating that this compound is mainly a competitive inhibitor under the experimental conditions used for the enzymatic assay.

3.2. Catalytic voltammetry with nitrate, chlorate and perchlorate

Like *Pp* NarGH [15] and *Ec* NarGHI [16], *Mh* NarGH is easily adsorbed onto the pyrolytic graphite electrode in the presence of neomycin. Because of the polar functionalities such as –COOH and –COH groups, hydrophobic areas present in the graphite, and the positively charged neomycin, the electrode works as a "combinatorial" surface where proteins can interact and bind [20]. These interaction forces are weak and usually do not affect the natural folding and activity of the enzyme [21]. In the case of *Mh* NarGH, the electrode surface mimics the membrane subunit NarI and the physiological redox partner, the quinone pool. By this way, the NarGH redox centers can be controlled by modulating the applied potential at the electrode surface, and the current-potential profile obtained in the presence of the substrate is the result of the variation of the enzyme catalytic activity as a response to the applied potential. This technique is known as protein film voltammetry (PFV) and is an effective method for real-time monitoring the catalytic performance of an enzyme [20,22,23]. The catalytic response becomes more consistent if the interfacial electron transfer ($1/i_E$) and the substrate mass transport ($1/i_{trans}$) are not limiting factors. When the inherent catalytic properties of the enzyme ($1/i_{cat}$) represent the slowest event in the process ($1/i_{lim}$~$1/i_{cat}$), the position, steepness, and shape of the catalytic wave correspond to intrinsic thermodynamic and kinetic properties of the enzyme, as well as its interaction with the substrate [24].

Cyclic voltammograms of *Mh* NarGH adsorbed onto a pyrolytic graphite disk electrode were recorded in the absence and presence of nitrate. In the absence of substrate non-turnover signals could not be detected, indicating that probably the electro-active coverage is very low. In the presence of nitrate a catalytic response was observed. The intensity of this catalytic signal increased with the substrate concentration reaching a maximum at 1 mM nitrate. Typical voltammograms with the background capacitance contribution

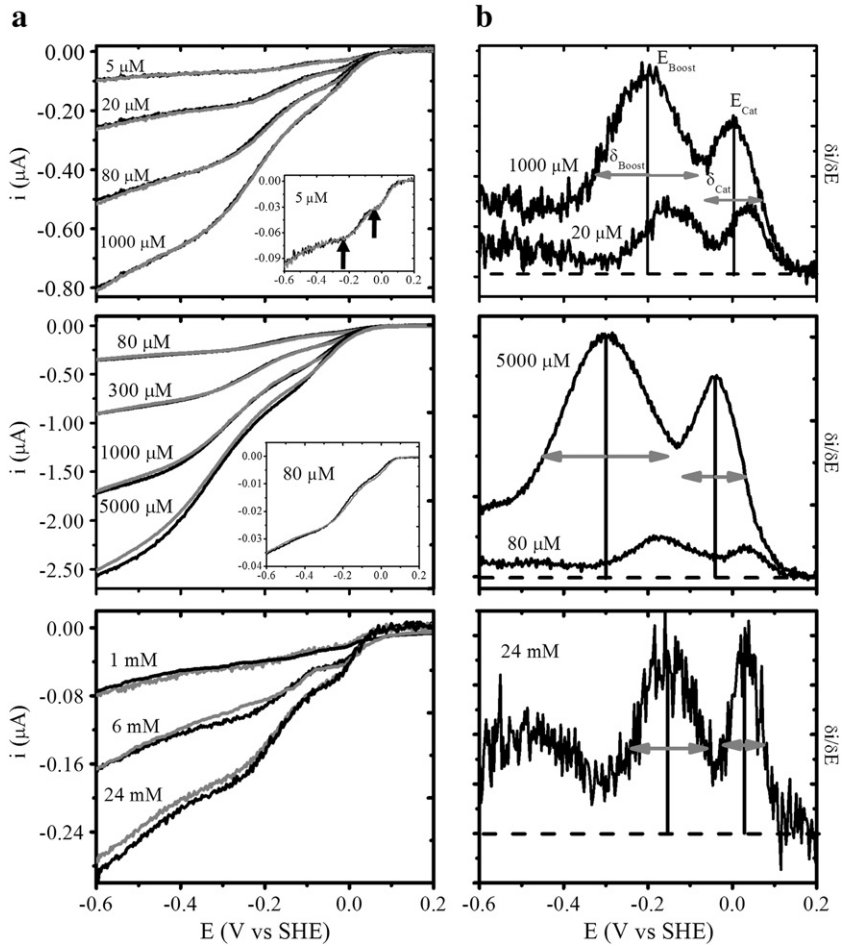

Fig. 2. (a) Catalytic responses of *Mh* 617 NarGH adsorbed on a pyrolytic graphite electrode in the presence of nitrate (top), chlorate (middle) and perchlorate (bottom). (b) First derivatives ($\delta i/\delta E$) of the voltammograms obtained with nitrate (top), chlorate (middle) and perchlorate (bottom). All the experiments were performed at room temperature and pH 7.60, at a scan rate of 20 mV/s and with the electrode rotated at 2000 rpm. Forward and backward scans are depicted in black and gray, respectively. A blank subtraction has been made.

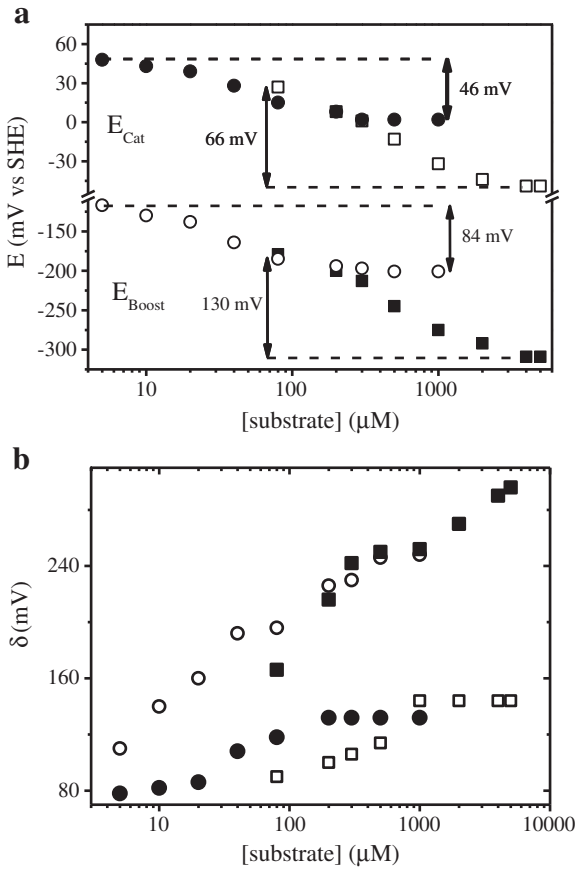

Fig. 3. (a) Variation of the position of E_{Cat} and E_{Boost} of the catalytic voltammograms with increasing nitrate (circles) and chlorate (squares) concentrations. (b) Variation of δ_{Cat} and δ_{Boost} with increasing nitrate (circles) and chlorate (squares) concentrations.

subtracted are shown in Fig. 2. After a careful analysis of the influence of the potential scan and electrode rotation rates, the values of 20 mV·s^{-1} and of 2000 rpm were chosen to guarantee independence from interfacial electron transfer and substrate mass transport rates. Neomycin was fundamental for the enzyme–electrode interaction since no stable film was obtained in the absence of this promoter. Voltammograms recorded in the ionic strength range from 0 up to 100 mM NaCl showed no significant differences.

As shown in Fig. 2a, the forward and reverse scans for nitrate reduction are superimposed, indicating the reversibility of the process. The catalytic responses for only a few substrate concentrations are illustrated in Fig. 2 for clarity. The shape of the catalytic wave of *Mh* NarGH is independent of the substrate concentration in the range 0.005–2 mM (K_M/4–100×K_M). The catalytic waveform for all nitrate concentrations is characterized by a small sigmoidal component at high redox potential (e.g., from 120 to −70 mV, inflection point, E_{Cat}, ca. 2 mV, for 1 mM nitrate), followed by a second sigmoidal component (activity boost) at lower potentials (e.g., from −70 to −400 mV, inflection point, E_{Boost}, ca. −201 mV, for 1 mM nitrate). It

Table 2
Maxima (E_{Cat} and E_{Boost}) and half-height widths (δ_{Cat} and δ_{Boost}) of the catalytic currents first derivatives obtained for nitrate, chlorate and perchlorate at saturating concentrations (1, 5 and 24 mM, respectively).

Substrate	E_{Cat} [mV]	δ_{Cat} [mV]	E_{Boost}[mV]	δ_{Boost} [mV]
NO_3^-	2	134	−201	260
ClO_3^-	−49	144	−309	293
ClO_4^-	32	90	−160	180

Table 3
K_M values for NO_3^-, ClO_3^- and ClO_4^- obtained by PFV. The K_M values are presented for the high- (E_{Cat}) and low-potential (E_{Boost}) activities. The competitive (K_{iC}) and uncompetitive (K_{iU}) inhibition constants of azide are also reported for both activity regions. nd, not determined.

NarGH	K_M [μM]	K_M [μM]	K_{iC} [μM]	K_{iU} [μM]	K_{iC} [μM]	K_{iU} [μM]
	Cat	Boost	(N_3^-) Cat		(N_3^-) Boost	
NO_3^-	36	56	0.06	3.35	0.03	9.24
ClO_3^-	820	822	nd	nd	nd	nd
ClO_4^-	1191	2276	nd	nd	nd	nd

is also evident that at redox potentials below −400 mV the catalytic current does not reach a plateau, but instead a residual slope is observed. The catalytic response was independent of product accumulation since nitrite addition to the electrolyte solution did not affect the voltammograms waveshape. A different behavior was particularly evident for the voltammograms obtained for *Pp* and *Ec* Nars at low nitrate concentrations (substrate-limiting conditions), since a catalytic current maximum was observed [15,16]. However, at high substrate concentrations (enzyme-limiting conditions) the bi-sigmoidal response obtained in *Mh* NarGH is similar to that observed in *Ec* NarGHI.

The electrochemical behavior of *Mh* NarGH was also investigated in the presence of chlorate and perchlorate using the same experimental conditions as for nitrate. The voltammograms for the three substrates were recorded using the same protein film due to its outstanding stability on the PG electrode. Film loss and enzyme denaturation were negligible since the catalytic signal in the presence of nitrate at the end of a set of experiments displayed identical current intensity and waveshape to the initial response. The waveshape of the catalytic voltammograms for both chlorate and perchlorate was similar to that observed for nitrate, i.e., the signals presented two sigmoidal components and a residual slope at more negative potentials (Fig. 2). However, significant differences were observed in the magnitudes of the catalytic currents (Fig. 2) and in the position of E_{Cat} and E_{Boost} (Fig. 3 and Table 2). Note that E_{Cat} and E_{Boost} were identified as E^1_{Cat} and E^2_{Cat} or E_{Switch} in [15,16].

The kinetic constants of an enzyme are usually obtained plotting the maximal catalytic current (i) at the plateau of the sigmoidal curve for each substrate concentration. In the case of *Mh* NarGH, the catalytic currents were measured at the potential corresponding to the end of each sigmoidal component, which depends on the substrate concentration (see inset of Fig. 2a). This method was chosen since i measured at a fixed potential value yielded incorrect K_M values. The data obtained for the three substrates were interpreted assuming a Michaelis–Menten model (Eq. (2), Fig. S2)

$$i = \frac{i_{Lim} \times C_{Substrate}}{K_M + C_{Substrate}} \quad (2)$$

The K_M values determined for the "Cat" and "Boost" processes for each substrate are reported in Table 3. The determination of turnover numbers from the limiting catalytic currents (i_{Lim}) was not possible from these PFV assays since *Mh* NarGH did not present non-turnover signals, preventing the determination of the electroactive coverage.

As can be seen in Table 3, the K_M values for both processes determined by PFV are considerably lower than those obtained through spectrophotometric assays for each substrate (Table 1). Similar differences have been observed for *Pp* NarGH and *Ec* NarGHI and were interpreted on the basis of the physical and chemical distinctions between the two types of assays [8,9,15,16]. Nevertheless, a similar trend of affinity between the enzyme and the different substrates was verified for spectrophotometric assays and PFV. Namely, in both the "Cat" and "Boost" processes, the i_{Max} and K_M values for chlorate are larger than those of nitrate. The i_{Lim} obtained for perchlorate

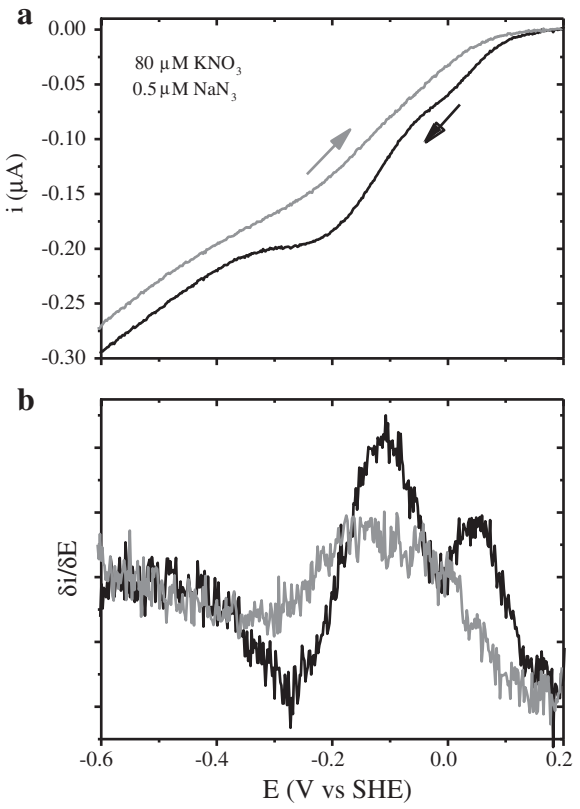

Fig. 4. (a) Cyclic voltammogram of *Mh* 617 Nar in the presence of 80 μM potassium nitrate and 0.5 μM sodium azide. Experimental conditions are the same as in Fig. 3. (b) Plot of the first derivative ($\delta i/\delta E$) of the voltammogram showed in (a). Forward and backward scans are depicted in black and gray, respectively.

were significantly smaller than those of nitrate and chlorate, while the K_M values were higher (Table 3).

Plotting the first derivative of the catalytic current with respect to applied potential ($\delta i/\delta E$ vs. E) is a useful method to highlight features in a cyclic voltammogram, namely the position and the steepness of the curve [15]. The first derivatives for nitrate, chlorate and perchlorate display two well-defined positive components representing the two different enzyme behaviors (Fig. 2b). The maximum of the peaks correspond to the midpoint redox potentials (E_{Cat} and E_{Boost}) of each catalytic event. For the three substrates analyzed, both E_{Cat} and E_{Boost} shifted to more negative potentials as the concentration increased. The variations observed for nitrate and chlorate are presented in Fig. 3a (data for perchlorate are not shown due to the low resolution of the first derivatives). The E_{Cat} values obtained at the lowest and highest concentrations of nitrate and chlorate differ in 46 and 66 mV, respectively. In the case of E_{Boost}, larger shifts of the values were observed, namely 84 mV for nitrate and 130 mV for chlorate. The shifting of both E_{Cat} and E_{Boost} with substrate concentration was also observed in *Pp* NarGH [15]. It is important to highlight that, despite the bi-sigmoidal waveshape being always observed independently from the substrate, the E_{Cat} and E_{Boost} values were remarkably affected by the type of substrate (Table 2), indicating that both redox events are related to the enzyme–substrate complex rather than to intrinsic properties of the free enzyme. In other words, enzyme–substrate complex formation occurs before any redox event.

The half-height width (δ) of the first derivative reflects the steepness of the corresponding catalytic wave and should enable the determination of the apparent number of electrons (n_{app}) involved in the process [22,25]. In particular, δ values of 90 and 45 mV are predicted for one- and two-electron transfer reactions, respectively. In the case of *Mh* NarGH, the δ values (δ_{Cat} and δ_{Boost} in Fig. 2b) span in the range 78–132 mV for E_{Cat} and 110–248 mV for E_{Boost}, in the case of nitrate (Fig. 3b). For chlorate, δ values in the range 90–144 mV for E_{Cat} and 166–296 mV for E_{Boost} were obtained (Fig. 3b). The δ values for both nitrate and chlorate are considerably larger than 45 mV, which is the value expected for the two-electron reduction, hindering an accurate calculation of the apparent number of electrons involved in the "Cat" and "Boost" processes. The high complexity of the system and the possible convolution of concerted electron transfer and coupled chemical events are probably responsible for this broadening. At the light of the present results and the explanations found in the literature it is impossible to draw any conclusion about the processes involved in the δ values broadening. Nevertheless, it is interesting to point out that, independently of the type and concentration of the substrate, the δ_{Boost} value is about twice that of δ_{Cat}. In addition, both δ_{Cat} and δ_{Boost} increase with substrate concentration, suggesting the existence of a substrate-dependent effect on the half-height widths not related to mass transfer limitation and to the mere number of electrons involved, which by itself should be independent from the substrate concentration.

3.3. Catalytic voltammetry in the presence of azide

The inhibition properties of azide in *Mh* NarGH were also analyzed by PFV. For increasing concentrations of azide, the intensity of the catalytic current decreased, confirming that the electrocatalytic profile observed in the absence of azide reflects features related to the enzyme active site reaction with the substrate. Concentrations above 5 μM produced a complete inhibition of the catalytic response, with the voltammogram being undistinguishable from that obtained with a nitrate-free solution. The same film of protein was then tested in a fresh nitrate-saturated electrolyte and the catalytic response was completely recovered (not shown), showing that azide is a reversible inhibitor of *Mh* NarGH. The inhibition effect was analyzed by varying the nitrate concentration between 5 and 2000 μM in the absence and in the presence of 0.5 and 2.0 μM sodium azide. Fig. 4a shows the current profile in the presence of 80 μM nitrate and 0.5 μM azide, which clearly evidences that both the high- and the low-potential activities are affected by the inhibitor. The first derivative of the catalytic wave highlights the different features of the forward and backward signals (Fig. 4b). The forward curve presents the profile described in Fig. 2, with two peaks corresponding to the inflection points of the high- and low-potential activities. In contrast, the backward catalytic wave is characterized by a single sigmoidal component, which does not superimpose the forward scan (Fig. 4a), with a first derivative

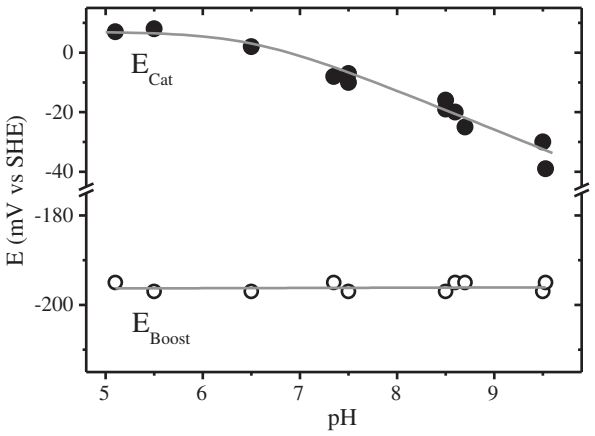

Fig. 5. Variation of E_{Cat} (black circles) and E_{Boost} (empty circles) with the pH. The electrolyte was composed by a mixture of 10 mM MES, 10 mM HEPES, 10 mM MOPS, 10 mM CAPS in order to vary the pH between 5.0 and 9.5. All the experiments were performed at room temperature at a scan rate of 20 mV/s and with the electrode rotated at 2000 rpm.

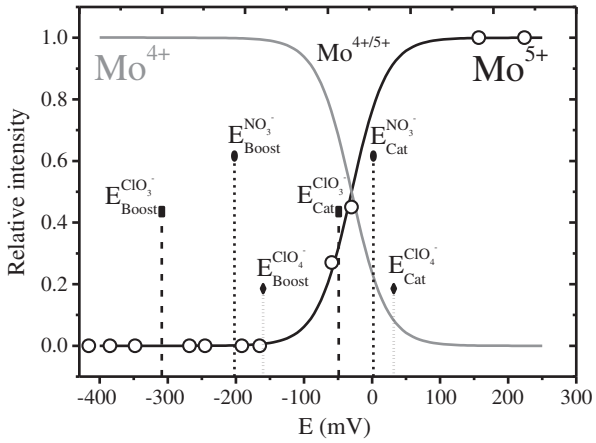

Fig. 6. EPR titration; variation of the Mo^{V} signal intensity (empty circles) with potential (vs. SHE). Black solid line is the nernstian fit of the experimental data assuming $E_m^{(V/IV)} = -30$ mV. Measurements conditions: microwave frequency, 9.65 GHz; temperature, 25 K; microwave power, 0.6 mW; modulation frequency, 10 kHz; modulation amplitude, 5 Gpp; buffer, 10 mM Tris–HCl pH 7.60.

characterized by a single broad peak (Fig. 4b). This profile was conserved after successive scans.

The type of inhibition and the respective inhibition constants can be determined through the analysis of the variation of the catalytic currents as a function of substrate concentrations for several concentrations of the inhibitor. The values reported in Table 3 were obtained using the Dixon and Cornish plots (Fig. S1b) and revealed that azide behaves as a competitive inhibitor for both the high- and the low-potential activities. This is in line with the spectrophotometric kinetics assays (see Section 3.1) and previous reports for *Ec* NarGHI, *Pp* NarGH and *Pd* NarGH [8,15,16]. For *Mh* NarGH, the K_{iU} / K_{iC} ratio is approximately 60 for the high potential activity (E_{Cat}) and 350 for the low-potential activity (E_{Boost}), indicating an increase in the competitive character of azide at lower potentials. It is also remarkable that the competitive constant K_{iC} at low potential is about half of that calculated for the high potential activity, suggesting a higher affinity of the inhibitor molecule to the reduced active site.

3.4. Catalytic voltammetry at different pH values

The catalytic voltammetric response of *Mh* NarGH at different pH values was analyzed using a nitrate concentration of 1 mM (substrate saturating conditions). A single *Mh* NarGH film yielded a catalytic response in the pH range 5.0–9.5, enabling the possibility to analyze the effect of the pH on the E_{Cat} and E_{Boost} values. As observed in *Ec* NarGHI [16], the catalytic current intensity increases at lower pH (not shown), indicating that the enzyme catalyzes more effectively the reduction of nitrate in mild acid media. This effect is not observed in the spectrophotometric activity assays (V_{max} constant between pH 6.0–8.0) likely due to the different nature of the experiment, i.e., the capability of the electron donor dithionite/methyl viologen might be negatively affected at lower pH. The E_{Cat} and E_{Boost} values were determined from the first-derivative plots ($\delta i/\delta E$) of the voltammograms at each pH assayed. Similar to *Ec* NarGHI [16], the E_{Cat} value shifts to more negative potentials (from 7 to −39 mV) as the pH becomes more alkaline, while the E_{Boost} remains constant at ca. −200 mV in the pH range 5.0–9.5 (Fig. 5). This confirms that E_{Boost} is not tuned by any acid–base transition in the range analyzed, whereas E_{Cat} is affected by a species subjected to an acid–base equilibrium. The experimental data was fitted using the same model as Elliot et al. ($E = E^{o} - {}^{o}(RT/nF) \times \ln\{1 + (K_{Ox}/[H^+])\}$) [16]. This model yield a pK_a^{Ox}~6.5, a value considerably lower than the $pK_a^{Ox} = 7.8$ reported for *Ec* NarGHI. In addition, an unexpected small slope was observed in the variation of the E_{Cat} vs. pH, which yield an $n = 4$. This value is not comparable to those obtained through the analysis of the δ values and then they cannot be correlated. At present we are not able to explain this behavior though, the dependence of E_{Cat} and E_{Boost} with pH in *Mh* NarGH is in agreement with that of *Ec* NarGHI [16].

3.5. EPR-mediated redox titration

An EPR redox titration was performed to evaluate the population distribution of the Mo oxidation states in the potential range in which the catalytic response of *Mh* NarGH was observed by PFV. The redox potential of the $Mo^{6+/5+}$ and $Mo^{5+/4+}$ couples were studied following the intensity of the EPR signal of the Mo(V) ion at pH 7.6 (Fig. 6), which was the pH used in our PFV experiments. It is important to mention that upon freezing, a solution buffered with Tris–HCl, pH 7.6, can increase its pH up to 9.0. Though, it was already demonstrated that this process does not affect the EPR signal in *Mh* Nar [10]. A representative EPR spectrum followed during the titration and its line shape dependence on pH variation from 7.6 to 9.0 is shown in Fig. S3. The intensity of the high-pH Mo(V) signal was essentially independent of the electrochemical potential across the range +50 to +250 mV, indicating that the reduction potential of the $Mo^{6+/5+}$ redox couple is higher than +250 mV and therefore out of the range analyzed by PFV. At potentials below −150 mV the Mo(V) EPR signal was no longer observable, indicating that the Mo(V) population was transformed into the EPR silent Mo^{4+} species. A least-squares fit to the data of the Mo(V) signal with a Nernstian function ($n = 1$) yielded $E = -30$ mV (Fig. 6). This value is similar to the E_{Cat} and considerably distant from the E_{Boost}.

Several authors that studied Mo enzymes through protein film voltammetry proposed that the two catalytic events observed in the voltammograms are related to the oxidation state of the Mo ion that will coordinate the substrate [15,16,26,27]. This conclusion was mainly supported by EPR-mediated spectropotentiometric titrations in which some authors found that the E_{Switch} value (named E_{Boost} for *Mh* NarGH) is similar to the reduction potential of the $Mo^{5+/4+}$ redox couple [27]. On this basis, the high potential activity (centered at E_{Cat}) was attributed to the interaction of the substrate with the Mo(V) ion, while the low potential activity (centered at E_{Switch} or E_{Boost}) was considered with the Mo(IV) ion [27].

The discrepancy between the redox potential of the $Mo^{5+/4+}$ couple and the $E_{Switch/Boost}$ was also observed in *Ec* NarGHI and *Pp* NarGH, suggesting that the model proposed by Anderson et al. [15] and Elliot et al. [16] would not be valid to explain the waveshape of the voltammograms of Nars. A more correct approach would be to determine the reduction potential of the Mo^{5+}-nitrate/Mo^{4+}-nitrate couple. However, this value cannot be determined by spectropotentiometry since adding dithionite or reduced methyl viologen to a *Mh* NarGH sample incubated with the substrate results in enzyme turnover yielding a Mo(V) EPR signal, which is different from that obtained by incubation in the absence of any reducing agent [10].

4. Discussion

Protein film voltammetry is a powerful tool to characterize the mechanism of redox enzymes. Under conditions where neither interfacial electron transfer nor substrate mass transport are limiting, the magnitude and shape of the catalytic current versus applied potential provide valuable information about intrinsic properties of the enzyme. *Mh* NarGH was adsorbed onto a pyrolytic graphite electrode surface to promote direct electron transfer between the electrode and the redox centers of the protein. The outstanding stability of the NarGH film allowed the use of the same film under different conditions, enabling a fast and precise evaluation of the enzyme performance as a function of pH and ionic strength, and its behavior toward different substrates and inhibitors. The catalytic activity in the potential domain revealed a complex response, composed by two sigmoidal components plus a residual slope at very negative

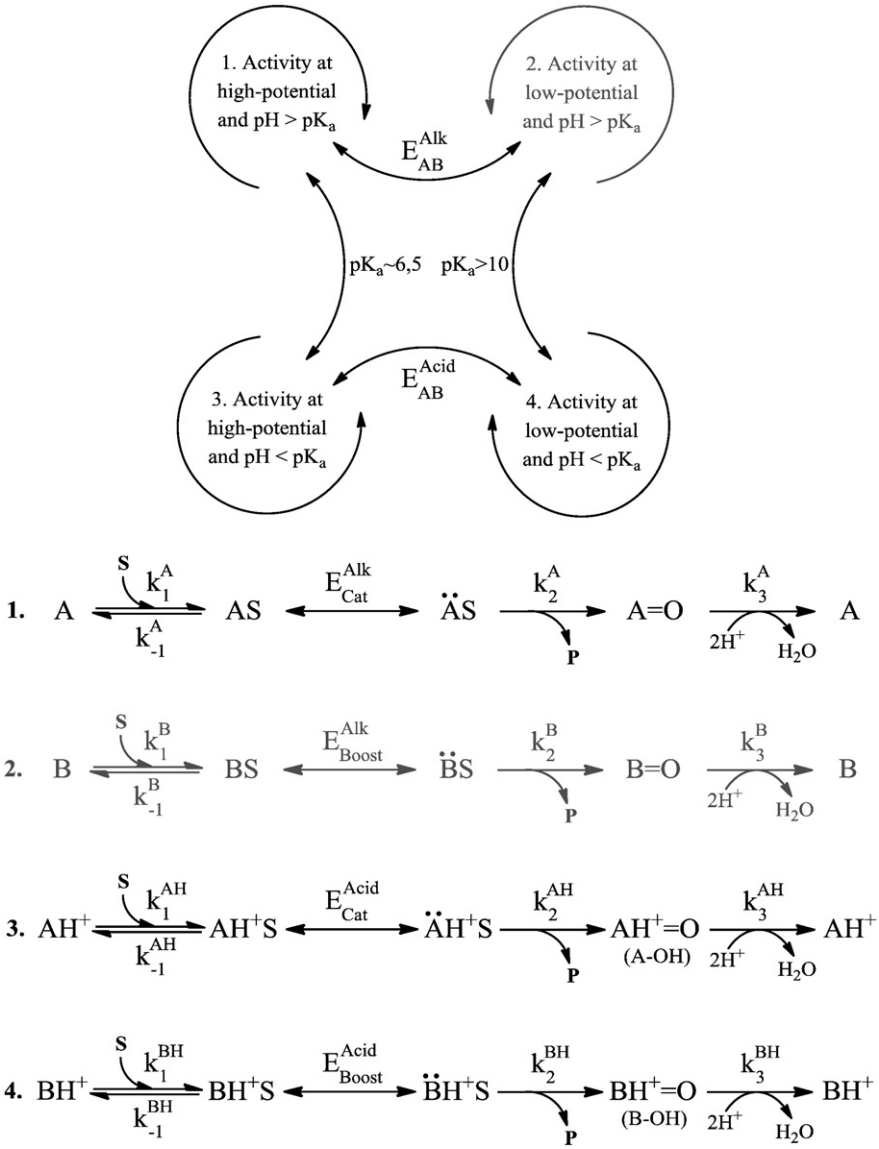

Scheme 2. Proposed reaction scheme for substrate reduction by *Mh* NarGH based on kinetic and voltammetric evidences. Gray arrows represent the pathway that is unlikely to occur given the high pK_a of the acid–base equilibrium of the enzyme form responsible for the low-potential activity.

redox potentials (Fig. 2). The catalytic behavior of *Mh* NarGH with nitrate, chlorate and perchlorate is in line with in-solution spectrophotometric kinetics assays using methyl viologen (reduced with sodium dithionite) as electron donor (Table 1 and 3). Both PFV and kinetic assays showed that nitrate is the substrate with the highest specificity, though chlorate showed higher turnover rates. In contrast, perchlorate as substrate displayed a very low affinity and reactivity (Tables 1 and 3); a fact that can be ascribed to the bulky nature of the perchlorate anion (tetrahedral) compared to nitrate (planar) and chlorate (pyramidal) anions. According to the E_{Cat} and E_{Boost} values obtained for the three substrates (perchlorate shows E values higher than nitrate and chlorate, Table 2) and the Arrhenius equation used in enzymology [28], the perchlorate reduction is thermodynamically more favorable but its higher activation energy makes the process kinetically unfavorable, as evidenced by the slower turnover rates.

4.1. The general model accepted for Mo enzymes

The catalytic voltammetric response of *Mh* NarGH is different from those reported for nitrate reductases of the DMSO reductase family of Mo enzymes [15,16,26,29–31]. *Ec* NarGHI and *Pp* NarGH showed a catalytic current waveform dependent on the substrate concentration [15,16]. At low nitrate concentration (substrate limiting condition) the voltammogram is characterized by a local maximum from which the catalytic current decreases at more negative potentials reaching a constant value (stationary phase). In contrast, at higher substrate concentration (enzyme limiting condition) the waveshape converts into a sigmoidal signal followed by a catalytic current boost at more negative potentials. Scheme 1 summarizes the reaction mechanism for these two enzymes showing the two kinetically distinct pathways. In this model, it was proposed that only Mo(V) and Mo(IV) can bind the substrate, and that the Mo(V) ion has a higher affinity for nitrate, as expected from the electrostatic repulsion between the nitrate anion and the more negatively charged Mo(IV) site. On this basis, at high potential and both at low and high concentrations, the Mo(VI) site would be reduced to Mo(V) because of the high redox potential of the $Mo^{6+/5+}$ couple (~400 mV). Then, nitrate coordinates to the Mo(V) ion and the catalysis continues with the addition of a further electron and two protons followed by product release. In contrast, at more negative potentials the electron transfer rate is higher and thus, at low nitrate concentrations, the Mo(VI) is

reduced to Mo(IV) before substrate binding. This results in a slower turnover rate (smaller catalytic current) because of the lower affinity of nitrate to the Mo(IV) ion compared to the Mo(V). However, at higher nitrate concentrations the different affinities for Mo(V) and Mo(IV) become negligible and both catalytic pathways occur, resulting in a catalytic boost in the case of *Ec* NarGHI [16]. In this case the rate of catalysis is enzyme limited and the two-sigmoidal response is observed. It is important to stress that in the case of *Pp* NarGH, Anderson et al. [15] assumed that under this condition a plateau was attained (rather than a boost), though the potential window was very narrow (between 0.4 V to −0.2 V) and the last part of the voltammogram clearly does not reach a stationary current value.

In contrast with the results reported for *Pp* NarGH and *Ec* NarGHI, the catalytic voltammograms of the *Mh* NarGH did not show any waveshape dependence on the substrate concentration, even though the substrate limiting conditions were guaranteed by starting at substrate concentrations six-, ten- and four-fold below the K_M of nitrate, chlorate and perchlorate, respectively (Table 3). The different catalytic waveshapes of *Mh* NarGH could be related to the different amino acid composition of the NarG subunit when compared to those of *Ec* and *Pp*. However, primary sequence alignments reveal that the three enzymes share 77% identity and the key amino acids at the active site are conserved. On the other hand, *Ec* DMSOr [27] and Naps [29,34] yield similar electrochemical responses, though they share very low sequence identity and have different substrate specificity. Based on this, it is difficult to correlate at present the amino acid composition with the catalytic waveshape of an enzyme. The only evidence found in the literature showed that the low potential current switch observed in the native *Rs* NapAB is replaced by a boost in the M153A mutant suggesting that changes in key amino acids would affect the catalytic waveshapes [32]. Surely, the production and study of *Mh* NarG site-directed mutants will help to address this issue.

As shown in Fig. 2, similar waveshapes were obtained for all substrates analyzed both at low and high concentrations. Taking into account the model of Scheme 1, the lack of local current maximum and the presence of a boost at low substrate concentration would imply that in *Mh* NarGH the Mo(IV)–substrate interaction is more efficient than the Mo(V)–substrate for the three substrates, which is counterintuitive based on electrostatic considerations. Moreover, the model of Scheme 1 does not take into account that nitrate, chlorate and perchlorate showed remarkable different catalytic potentials (E values) that tend to shift toward more negative values once the substrate concentration is increased (Anderson et al. [15] reported that voltammograms obtained with *Pp* NarGH and chlorate as substrate yielded E_{Cat} values slightly different from those obtained with nitrate, but owing to the small difference no conclusions were drawn). The model proposed as explanation to the *Ec* NarGHI and *Pp* NarGH catalytic response relates both E_{Cat} and $E_{Switch/Boost}$ to the molybdenum oxidation state but does not consider the substrate interaction with the Mo site. Based on the EPR redox titration and the voltammetric data, our results are in agreement with the fact that when the potential scan is started in the PFV experiment, a Mo(V) ion might be present at the enzyme active site (Fig. 6). Elliot et al. [16] already showed that electrons could flow through the enzyme in the absence of substrate, as non-turnover signals were observed for *Ec* NarGHI through SWV, which led these authors to conclude that active site reduction might happen before substrate binding. However, this is in contrast with our results, which clearly demonstrates that the E_{Cat} and E_{Boost} values are tuned by the nature of the ligand interacting with the active site, indicating that the addition of the electrons needed to complete the reaction happens after substrate binding both in the "Cat" and the "Boost" processes. Therefore, E_{Cat} and E_{Boost} are the reduction potentials of two Mo–substrate complexes, which are somehow different in terms of geometrical and/or electronic configuration of the active site for the different substrates. These species are interchangeable and dependent on the applied potential. A similar model was proposed by Anderson et al. [15] to explain the different potential-dependent turnover rate based on the midpoint potential of a redox center rather than the active site. However, this would not explain the dependence of the $E_{Switch/Boost}$ value on the substrate concentration (and type in the case of *Mh* NarGH).

The order of addition where the substrate binds the active site first and then electrons are transferred from the electron donor has already been proposed in early kinetic studies performed in *Ec* NarGHI and *Pd* NarGHI [8,9]. The authors proposed that using viologen dyes as electron donor and nitrate as electron acceptor the enzyme follows a Theorell–Chance mechanism (i.e., compulsory order with no significant accumulation of ternary complexes) in which nitrate binding to the enzyme is required to promote the electron transfer from the donor to the active site. Instead, when quinols were used as electron donor, the nitrate reduction was more consistent with a two-site enzyme substitution mechanism, where the sequence of substrates addition is the same but accumulation of ternary complexes is now significant. These evidences together with our results indicate that the scheme used to model the voltammograms of *Ec* NarGHI and *Pp* NarGH (Scheme 1) has some flaws, mainly in the Switch/Boost process, where the two electrons needed for substrate reduction are transferred before the binding of the substrate. In agreement with these kinetic studies, EPR data from *Ec* NarGHI [33] and *Mh* NarGHI (not shown) identified different Mo(V) signals when native Nar (i.e., as-isolated in aerobic conditions) is incubated in the presence of nitrate, chlorate or perchlorate. This indicates different Mo coordination environments and also suggests that these compounds can access to the active site prior to any redox event.

4.2. Alternative proposal for substrate reduction by Nars

On the basis of all the evidences discussed above, we propose a different model (Scheme 2) to explain the two-components observed in the catalytic voltammograms, as well as the dependence of the E values on both the pH and the substrate (nature and concentration). In order to elaborate a more general scheme, we will not associate any species to the oxidation states of the Mo ion; instead we will label them as A and B. The species A would be responsible for the process denoted as "Cat" while species B for the "Boost."

The alternative model implies that a reversible redox event switches between two catalytically distinct species A and B. These two forms of Nar have different k_{Cat} and affinity for the substrate. Anderson et al. [15] already proposed this model but, since their catalytic voltammograms recorded in the presence of nitrate or chlorate were very similar (both in waveshape and E values), they assumed that the electrochemical modulations of *Pp* NarGH activity occur independently of substrate-specific interactions within the active site. In contrast to this and as mentioned in Section 3.2, we were able to observe that both E_{Cat} and E_{Boost} values are remarkably affected by the nature of the substrate, indicating that the enzyme–substrate complex formation must occur before any redox event. In other words, this implies that the redox switch would occur between species AS and BS at high pH and between species AH^+S and BH^+S at low pH. It is important to highlight that the redox switch proposed in our model occurs only under catalytic conditions and then, should not be related to the redox potential of the Nar cofactors.

The center of Scheme 2 depicts the redox equilibrium between the enzymes forms responsible for the activity at high and low potentials, as well as the acid–base transition to which they can be subjected depending on the pH. The pK_a^A explain the pH dependence of the E_{Cat} value (Fig. 5) and means that species A can be protonated at pH below ~6.5. Since no pH dependence of E_{Boost} was observed (Fig. 5), the pK_a^B might be above the pH range studied in our work. A $pK_a^B > 10$ would imply that species B are immediately protonated upon redox switch between the high potential activity to the low potential activity and then, that the low potential activity is carried out only through the protonated form.

The reaction mechanism through any of the three possible pathways (starting in $X = A$, AH^+ or BH^+) implies that the enzyme binds the substrate forming, for example, AS (rate dependent on [S], k_1 and k_{-1}). Substrate binding triggers the transfer of the electrons needed to catalyze the oxygen-atom transfer reaction $\text{ÄS} \rightarrow A = O + P$ (rate dependent on k_2). This effect was clearly observed in the monomeric periplasmic nitrate reductase (NapA) from *Desulfovibrio desulfuricans* ATCC 27774 (*Dd*). When *Dd* NapA was incubated with reduced MV, neither the 4Fe-4 S cluster nor the Mo(VI) ion were reduced, despite of the low redox potential of the electron donor (−420 mV) being enough to reduce at least the FeS center (−390 mV). Addition of nitrate triggered the oxidation of MV indicating that substrate interaction with the active site was needed to enable electron transfer through the enzyme [34,35].

After product release, the species A = O needs to be protonated (rate dependent on k_3) to release a water molecule and regenerate the enzyme to the initial state A. The fact that the current intensities of both the "Cat" and "Boost" processes increase at lower pH (not shown) might indicate that protonation of the oxo-group bound to the active site affects the global reaction rate. The same behavior was observed in *Ec* NarGHI (Fig. 3 of reference [16]). The more likely explanation is that at lower pH more protons are available to catalyze the protonation, leading to the dehydration and regeneration of the enzyme to the starting state, which depends on the applied potential and pH.

4.3. Inhibition studies

Both in-solution kinetic assays and PFV studies indicated that azide is a competitive inhibitor of *Mh* NarGH. The voltammograms recorded at 20 mV/s showed hysteresis/irreversibility (Fig. 4a), which is best observed in the first-derivative of the catalytic current that clearly evidences the differences between the forward and the backward catalytic currents (Fig. 4b). This behavior may indicate that the affinity of azide for the low potential form of the Mo active site is stronger than for the high potential form, in agreement with the magnitude of the competitive inhibition constants obtained for the high and low potential catalyses, where it was observed that K_{iC} for the "Cat" process is twice that of the "Boost." A rather different interpretation was given for *Ec* NarGHI [16], in which it was proposed that azide has more affinity for the active site of the high potential catalytic activity. The reason behind this difference is striking, and might be due to the different analysis of the kinetic data performed by the authors.

4.4. Use of PFV to understand the physiological behavior of Nars

The steady-state kinetic and PFV data are in line with earlier in-solution kinetic studies performed by Boxer et al. [9]. The comparison between the two data sets allowed us to draw some interesting conclusions about how differently the two methodologies can affect the enzyme kinetics. Boxer et al. [9] carried out in-solution kinetic studies using both the heterotrimer (NarGHI) and the heterodimer (NarGH) testing two different electron donors: reduced methyl viologen (MV) and duroquinol (DQ) which is similar to the physiological electron donor menaquinol. Inhibition studies suggested that MV can directly reduce the molybdenum active site, while the quinols can only interact with the quinol-binding site present in the subunit NarI. The different interactions of MV and DQ yielded considerably different kinetic constants. The Michaelis constant obtained by Boxer et al. [9] using MV is very similar to the K_M of *Mh* NarGH using the same electron donor (*Ec* NarGHI $K_M^{MV} = 420\ \mu M$, *Mh* NarGH $K_M^{MV} = 225\ \mu M$). More interestingly, the K_M obtained by PFV is of the same order of magnitude of that reported by Boxer et al. [9] using DQ as electron donor, and very different from the constant determined using MV (*Ec* NarGHI $K_M^{DQ} = 2\ \mu M$, *Mh* NarGH $K_M^{PFV} = 36\ \mu M$, Table 3). Similar results were observed by Craske et al. [8] for the *Pd* Nar GHI ($K_M^{MV} = 283\ \mu M$ and $K_M^{DQ} = 13\ \mu M$). These evidences lead us to consider again the kinetic model proposed by Boxer et al. [9] and, for the first time, to assert that the different kinetic parameters obtained by in-solution kinetics and PFV (observed for many others systems before [15,16]), are likely due to different mechanisms related to the nature of the reducing substrate rather than simple effects related to the technique. In this scenario, the graphite electrode is confirmed to play a role similar to that of the physiological donor, driving to kinetic constants close to the physiological ones. On the other side, MV is established to be far from being physiological and it is clear how its action on the redox centers is random. This is supported by studies performed by Buc et al. [36] on *Ec* NarGH that demonstrated how the reduced MV can directly reduce all four Fe–S centers and the Mo cofactor. If not taken into consideration, the reducing substrate can lead to an easy misinterpretation of the enzyme kinetic properties.

5. Concluding Remarks

In the present paper is reported the first study where very different E_{Cat} and E_{Boost} values are obtained for alternative substrates, indicating that electrochemical modulations of the activity of *Mh* NarGH depends on substrate-specific interactions within the active site. This contradicts the models proposed by Anderson et al. [15] and Elliot et al. [16] for *Pp* NarGH and *Ec* NarGHI, respectively. The model on Scheme 1 could explain that the substrate interaction affects the E_{Cat} value. However, the fact that the two electrons needed to catalyze the substrate reduction in the "Switch/Boost" process are transferred before substrate binding, would not affect its position.

Based on our results and earlier kinetic and spectroscopic evidences [8,9,33] we proposed a model that explains the two-sigmoidal waveshapes of the catalytic voltammograms and their dependence on the type of substrate and the pH used in the assay.

It is clear that these enzymes are far from being completely understood. For instance, the unexpected large δ values observed in the first-derivative of the catalytic voltammograms, which should be indicative of the electrons involved in the catalysis, as well as their dependence on both substrate concentration and nature (Fig. 3b) cannot be explained at present and deserves further investigation.

Supplementary data related to this article can be found online at doi:10.1016/j.bbabio.2012.04.011.

Acknowledgments

J.M. thanks Fundação para a Ciência e a Tecnologia (FCT) for the fellowship (SFRH/BD/60725/2009) and Célia M. Silveira for technical support. P.M.P.S. and P.J.G. thank programs Ciência 2007 and Ciência 2008 of FCT for funding. This work has been supported by FCT through grant no. PEst-C/EQB/LA0006/2011. C.D.B. is a member of CONICET (Argentina).

References

[1] D.J. Richardson, Bacterial respiration: a flexible process for a changing environment, Microbiology 146 (2000) 551–571.
[2] P.J. Gonzalez, C. Correia, I. Moura, C.D. Brondino, J.J. Moura, Bacterial nitrate reductases: molecular and biological aspects of nitrate reduction, J. Inorg. Biochem. 100 (2006) 1015–1023.
[3] M. Jormakka, B. Byrne, S. Iwata, Protonmotive force generation by a redox loop mechanism, FEBS Lett. 545 (2003) 25–30.
[4] J.J. Moura, C.D. Brondino, J. Trincao, M.J. Romao, Mo and W bis-MGD enzymes: nitrate reductases and formate dehydrogenases, J. Biol. Inorg. Chem. 9 (2004) 791–799.
[5] W.G. Zumft, Cell biology and molecular basis of denitrification, Microbiol. Mol. Biol. Rev. 61 (1997) 533–616.
[6] A.L. Ballard, S.J. Ferguson, Respiratory nitrate reductase from Paracoccus denitrificans. Evidence for two b-type haems in the gamma subunit and properties of a water-soluble active enzyme containing alpha and beta subunits, Eur. J. Biochem. 174 (1988) 207–212.
[7] C.H. MacGregor, C.A. Schnaitman, D.E. Normansell, M.G. Hodgins, Purification and properties of nitrate reductase from *Escherichia coli* K12, J. Biol. Chem. 249 (1974) 5321–5327.

[8] A. Craske, S.J. Ferguson, The respiratory nitrate reductase from Paracoccus denitrificans. Molecular characterisation and kinetic properties, Eur. J. Biochem. 158 (1986) 429–436.
[9] F.F. Morpeth, D.H. Boxer, Kinetic analysis of respiratory nitrate reductase from *Escherichia coli* K12, Biochemistry 24 (1985) 40–46.
[10] C. Correia, S. Besson, C.D. Brondino, P.J. Gonzalez, G. Fauque, J. Lampreia, I. Moura, J.J. Moura, Biochemical and spectroscopic characterization of the membrane-bound nitrate reductase from Marinobacter hydrocarbonoclasticus 617, J. Biol. Inorg. Chem. 13 (2008) 1321–1333.
[11] R.A. Rothery, M.G. Bertero, R. Cammack, M. Palak, F. Blasco, N.C. Strynadka, J.H. Weiner, The catalytic subunit of *Escherichia coli* nitrate reductase A contains a novel [4Fe-4 S] cluster with a high-spin ground state, Biochemistry 43 (2004) 5324–5333.
[12] R.A. Rothery, M.G. Bertero, T. Spreter, N. Bouromand, N.C. Strynadka, J.H. Weiner, Protein crystallography reveals a role for the FS0 cluster of *Escherichia coli* nitrate reductase A (NarGHI) in enzyme maturation, J. Biol. Chem. 285 (2010) 8801–8807.
[13] M.G. Bertero, R.A. Rothery, M. Palak, C. Hou, D. Lim, F. Blasco, J.H. Weiner, N.C. Strynadka, Insights into the respiratory electron transfer pathway from the structure of nitrate reductase A, Nat. Struct. Biol. 10 (2003) 681–687.
[14] M. Jormakka, D. Richardson, B. Byrne, S. Iwata, Architecture of NarGH reveals a structural classification of Mo-bisMGD enzymes, Structure 12 (2004) 95–104.
[15] L.J. Anderson, D.J. Richardson, J.N. Butt, Catalytic protein film voltammetry from a respiratory nitrate reductase provides evidence for complex electrochemical modulation of enzyme activity, Biochemistry 40 (2001) 11294–11307.
[16] S.J. Elliott, K.R. Hoke, K. Heffron, M. Palak, R.A. Rothery, J.H. Weiner, F.A. Armstrong, Voltammetric studies of the catalytic mechanism of the respiratory nitrate reductase from *Escherichia coli*: how nitrate reduction and inhibition depend on the oxidation state of the active site, Biochemistry 43 (2004) 799–807.
[17] P. Baumann, L. Baumann, The marine Gram-negative Eubacteria: genera *Photobacterium*, *Beneckea*, *Alteromonas*, *Pseudomonas*, and *Alcaligenes*, in: M.P. Starr, H. Stolp, H.G. Trüper, A. Balows, H.G. Schlegel (Eds.), The prokaryotes. A handbook on Habitats, Isolation and Identification of Bacteria, Springer-Verlag, New York, 1981, pp. 1302–1331.
[18] R.L. Starkey, A study of spore formation and other morphological characteristics of *Vibrio desulfuricans*, Arch. Mikrobiol. 8 (1938) 268–304.
[19] A.J. Bard, L.R. Faulkner, Electrochemical Methods: Fundamentals and Applications, 2nd Edition Wiley, New York, 2001.
[20] C. Leger, S.J. Elliott, K.R. Hoke, L.J.C. Jeuken, A.K. Jones, F.A. Armstrong, Enzyme electrokinetics: Using protein film voltammetry to investigate redox enzymes and their mechanisms, Biochemistry 42 (2003) 8653–8662.
[21] F.A. Armstrong, R. Camba, H.A. Heering, J. Hirst, L.J. Jeuken, A.K. Jones, C. Leger, J.P. McEvoy, Fast voltammetric studies of the kinetics and energetics of coupled electron-transfer reactions in proteins, Faraday Discuss. (2000) 191–203.
[22] F.A. Armstrong, H.A. Heering, J. Hirst, Reactions of complex metalloproteins studied by protein-film voltammetry, Chem. Soc. Rev. 26 (1997) 169–179.
[23] C. Leger, P. Bertrand, Direct electrochemistry of redox enzymes as a tool for mechanistic studies, Chem. Rev. 108 (2008) 2379–2438.
[24] J.N. Butt, F.A. Armstrong, Voltammetry of adsorbed redox enzymes: mechanisms in the potential dimension, in: O. Hammerich, J. Ulstrup (Eds.), Bioinorganic Electrochemistry, Springer, Dordrecht (The Netherlands), 2008, pp. 91–128.
[25] J. Hirst, Elucidating the mechanisms of coupled electron transfer and catalytic reactions by protein film voltammetry, BBA-Bioenergetics 1757 (2006) 225–239.
[26] B. Frangioni, P. Arnoux, M. Sabaty, D. Pignol, P. Bertrand, B. Guigliarelli, C. Leger, In Rhodobacter sphaeroides respiratory nitrate reductase, the kinetics of substrate binding favors intramolecular electron transfer, J. Am. Chem. Soc. 126 (2004) 1328–1329.
[27] K. Heffron, C. Leger, R.A. Rothery, J.H. Weiner, F.A. Armstrong, Determination of an optimal potential window for catalysis by E. coli dimethyl sulfoxide reductase and hypothesis on the role of Mo(V) in the reaction pathway, Biochemistry 40 (2001) 3117–3126.
[28] A. Cornish-Bowden, Fundamentals of Enzyme Kinetics, 3rd ed. Portland Press, London, 2004.
[29] S.J. Field, N.P. Thornton, L.J. Anderson, A.J. Gates, A. Reilly, B.J. Jepson, D.J. Richardson, S.J. George, M.R. Cheesman, J.N. Butt, Reductive activation of nitrate reductases, Dalton Trans. (2005) 3580–3586.
[30] P. Bertrand, B. Frangioni, S. Dementin, M. Sabaty, P. Arnoux, B. Guigliarelli, D. Pignol, C. Leger, Effects of slow substrate binding and release in redox enzymes: theory and application to periplasmic nitrate reductase, J. Phys. Chem. B 111 (2007) 10300–10311.
[31] A.J. Gates, D.J. Richardson, J.N. Butt, Voltammetric characterization of the aerobic energy-dissipating nitrate reductase of *Paracoccus pantotrophus*: exploring the activity of a redox-balancing enzyme as a function of electrochemical potential, Biochem. J. 409 (2008) 159–168.
[32] V. Fourmond, B. Burlat, S. Dementin, M. Sabaty, P. Arnoux, E. Etienne, B. Guigliarelli, P. Bertrand, D. Pignol, C. Leger, Dependence of catalytic activity on driving force in solution assays and protein film voltammetry: insights from the comparison of nitrate reductase mutants, Biochemistry 49 (2010) 2424–2432.
[33] F.F. Morpeth, D.H. Boxer, R.C. Bray, G.N. George, Anion binding to the molybdenum centre of nitrate reductase from *Escherichia coli*, in: J.R. Dilworth, M.F. Lappert (Eds.), Some Recent Developments in the Chemistry of Chromium, Molybdenum and Tungsten, Royal Society of Chemistry (Dalton), London, 1983, 10 pp.
[34] P.J. Gonzalez, M.G. Rivas, C.D. Brondino, S.A. Bursakov, I. Moura, J.J. Moura, EPR and redox properties of periplasmic nitrate reductase from Desulfovibrio desulfuricans ATCC 27774, J. Biol. Inorg. Chem. 11 (2006) 609–616.
[35] S. Najmudin, P.J. González, J. Trincão, C. Coelho, A. Mukhopadhyay, N.M. Cerqueira, C.C. Romão, I. Moura, J.J.G. Moura, C.D. Brondino, M.J. Romão, Periplasmic Nitrate Reductase Revisited: A Sulfur Atom completes the Sixth Coordination of the Catalytic Molybdenum, J. Biol. Inorg. Chem. 13 (2008) 737–753.
[36] J. Buc, C.L. Santini, F. Blasco, R. Giordani, M.L. Cardenas, M. Chippaux, A. Cornish-Bowden, G. Giordano, Kinetic studies of a soluble alpha beta complex of nitrate reductase A from *Escherichia coli*. Use of various alpha beta mutants with altered beta subunits, Eur. J. Biochem. 234 (1995) 766–772.